Scattering from a partially fluid-filled, elastic-shelled sphere

J. A. Fawcett
Defence Research Establishment Atlantic, PO Box 1012, Dartmouth, Nova Scotia B2Y 3Z7, Canada

(Received 29 June 2000; revised 30 October 2000; accepted 15 November 2000)

In this article a sphere is taken to be partially filled with fluid so that its interior is part fluid and part air. A set of basis of functions, based upon an origin at the fluid/air interface, is used for the interior and a set of basis functions based upon the center of the sphere is used for the shell and exterior of the sphere. These sets of basis functions are coupled at the shell/interior interface and the resulting coupled system of equations solved to yield the scattered field. Numerical computations using this approach are presented for varying amounts of fluid-fill and for varying incident plane waves. [DOI: 10.1121/1.1339827]

PACS numbers: 43.30.Gv, 43.40.Fz [DLB]

I. INTRODUCTION

The modeling of acoustic scattering from an elastic-shelled sphere, either evacuated or filled, has been studied previously by a variety of authors.[1–4] In this article we describe an approach to modeling scattering from a partially filled elastic-shelled sphere. A schematic of a partially filled sphere is shown in Fig. 1. The partially filled interior introduces two interesting effects: (1) the monostatic scattering is no longer symmetric as a function of the angle off vertical and (2) there is an additional flat interface within the interior of the sphere which can cause enhanced scattering.

We start by assuming that the theory for scattering from a sphere with a homogeneous interior is well understood. The case of a partially filled sphere is then considered. The standard spherical harmonic series is assumed for the shell and exterior of the sphere. Another basis set (constructed from spherical harmonics) based with respect to the center of the interior air/water interface is used for the interior. These two basis sets are then coupled through the continuity equations at the shell/interior interface. Since these interface equations have an infinite number of coupled terms, they must be truncated in order to yield a numerically solvable system. Hence, unlike the standard spherical scattering problem it is not possible to write down an explicit numerical solution for the various functional coefficients in terms of simple determinants.[3,4]

From the derived set of scattering equations, numerical computations are performed showing the spectral characteristics for various amounts of fluid (we consider water) and corresponding pulse computations. These computations are done for a plane wave incident along the z axis. We conclude with a computation of the monostatic scattering strength as a function of the off-axis angle for a fixed amount of fill and fixed frequency.

II. THEORY

Let us first consider the case of a plane wave incident along the z axis so that the wavefield solution possesses azimuthal symmetry. We use the spherical coordinate system (R,θ,ϕ) where R is the three-dimensional radius, θ is the angle measured from the z axis and ϕ is the projection of the position vector in the x-y plane. Then we can write for the particle displacement $\vec{u}$ that

$$\vec{u}=-\nabla\Phi+\nabla\times\vec{\Psi}, \tag{1}$$

where Φ is a scalar compressional potential and $\vec{\Psi}$ is the vector shear potential. We will take

$$\vec{\Psi}=\nabla\times(\hat{e}_r\Psi). \tag{2}$$

Our basic building block for both Φ and Ψ is the solution to the Helmholtz equation in spherical coordinates:

$$P_n^m(\cos\theta)f_n(kR)e^{im\phi}, \tag{3}$$

where P_n^m are the Legendre polynomials, $f_n(kR)$ is either a spherical Bessel or Hankel function of order n, and k is the wave number depending upon the medium and the wave type (i.e., compressional or shear). Now for the sphere (shell and a homogeneous interior) and the exterior surrounding fluid, at a fixed azimuthal order m, the unknown potentials can be expressed as a sum over the components with the index $n \geqslant m$, the nth components having the form

$$\Phi_e=a_1^n h_n(k_e^p R)P_n^m(\cos\theta), \tag{4}$$

$$\Phi_{sh}=(a_2^n h_n(k_{sh}^p R)+a_3^n j_n(k_{sh}^p R))P_n^m(\cos\theta), \tag{5}$$

$$\Psi_{sh}=(a_4^n h_n(k_{sh}^s R)+a_5^n j_n(k_{sh}^s R))P_n^m(\cos\theta), \tag{6}$$

$$\Phi_{in}=a_6^n j_n(k_{in}^p R)P_n^m(\cos\theta). \tag{7}$$

Here we have used the notation that e denotes exterior, sh denotes shell and in denotes the interior. There are thus six unknown coefficients (a_i^n) and there are eight conditions to be satisfied (four at the outer and four at the inner interface), namely, for example, at the inner shell/interior interface:

$$u_r^{sh}=u_r^{in}, \tag{8}$$

$$\sigma_{rr}^{sh}=\sigma_{rr}^{in}, \tag{9}$$

$$\sigma_{r\theta}^{sh}=0, \tag{10}$$

$$\sigma_{r\phi}^{sh}=0. \tag{11}$$

However, some analysis shows that the fourth equation is satisfied if the third equation is satisfied; hence we only use

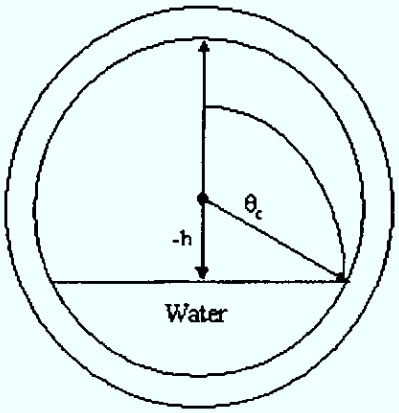

FIG. 1. A schematic of the cross-section of a partially filled shelled sphere.

the first three equations at each interface. At the shell/interior interface (and also at the exterior interface) we can write any of the equations (8)–(11) in the generic form (truncated at $n=N$),

$$\sum_{n=m}^{N} c_n P_n^m(\cos\theta)=\sum_{n=m}^{N} d_n P_n^m(\cos\theta), \tag{12}$$

where the right-hand side may, in fact, be equal to zero. In Eq. (12) the coefficients c_n and d_n represent all the nonazimuthal terms at order (m,n) lumped together, including various combinations of Bessel and Hankel functions and their derivatives and the unknown coefficients a_i^n of Eqs. (5)–(7). The equations for $\sigma_{r\theta}$ in fact involve the derivatives of the Legendre polynomials, but this condition can be integrated with respect to θ to yield the equivalent condition in terms of $P_n^m(\cos\theta)$.

For a shelled sphere with a homogeneous fluid interior, one just equates each term in Eqs. (8)–(10) at the shell/interior interface [which are of the form of Eq. (12)] to yield three of the equations of a 6×6 system for each order n (the other three equations come from the exterior water/shell interface). However, below where we consider the interior not to be homogeneous with respect to θ (i.e., there is an interior water/air interface), we will see that it is no longer possible to just simply equate terms in the series solution.

Let us now consider the interior of the sphere to be partially filled with fluid ($\theta_c<\theta<\pi$) and, as an example, consider in detail Eq. (9). For the unfilled portion we set $\sigma_{rr}=0$. For $\theta_c<\theta<\pi$ the interior is fluid with parameters c_1 and ρ_1. Within this fluid we consider an expansion based upon the center of the fluid/air interface (the coordinate $\tilde{\theta}=\pi/2$ along the interface); in particular, for the mth azimuthal order, we use the expansion for the interior, fluid compressional potential

$$\Phi_f=\sum_{n=m}^{N} a_6^n j_{q(n)}(k\tilde{R})P_{q(n)}^m(\cos\tilde{\theta}), \tag{13}$$

where $q\equiv m+2(n-m+1)-1$ and the a_6^n are the expansion coefficients [of the form of Eq. (7)] to be determined. The integer q represents the odd indicies after the first index which is $n=m$ (for example, for $m=0$, $q=1,3,5,7$, etc.). Substituting the expression $q\equiv m+2(n-m+1)-1$ into the relation that

$$P_q^m(0)\propto\cos\left(\frac{\pi}{2}(q-m)\right), \tag{14}$$

we find that with this choice of q, $P_q^m(\cos\tilde{\theta})=0$ for $\tilde{\theta}=\pi/2$ and thus the boundary condition $\Phi_f=0$ is automatically satisfied at the fluid/air interface.

In Eq. (13) the coordinates $\tilde{R}$ and $\tilde{\theta}$ represent the radius and the polar angle based upon the origin at the center of the fluid/air interface ($z=z_I$) and are given by

$$\tilde{R}(\theta)\equiv\sqrt{R^2\sin^2\theta+(R\cos\theta-z_I)^2} \tag{15}$$

and

$$\tilde{\theta}(\theta)\equiv\cos^{-1}\left(\frac{R\cos-z_I}{\sqrt{R^2\sin^2\theta+(R\cos\theta-z_I)^2}}\right), \tag{16}$$

where $R\equiv a$ along the shell/interior interface.

Now consider the equation for σ_{rr} at the inner interface. We have that

$$0=\sum_{n=m}^{N}(t(n)_1+t(n)_2+t(n)_2+t(n)_3+t(n)_4)P_n^m(\cos\theta), \tag{17}$$

$$\sum_{n=m}^{N}-\rho_1\omega^2 a_6^n j_{q(n)}(k\tilde{R})P_{q(n)}^m(\cos\tilde{\theta})=\sum_{n=m}^{N}(t(n)_1+t(n)_2+t(n)_3+t(n)_4)P_n^m(\cos\theta), \tag{18}$$

where Eq. (17) is valid in the angular range $0<\theta<\theta_c$ and Eq. (18) in the range $\theta_c<\theta<\pi$. The functions $t(n)_i$ represent the terms involving the shear and compressional potentials in the shell for the spherical Bessel functions j_n and h_n. We now multiply Eq. (18) by $\sin(\theta)P_\nu^m(\cos\theta)n_\nu$, where n_ν is a normalizing factor, and integrate with respect to θ to obtain

$$(t(\nu)_1+t(\nu)_2+t(\nu)_3+t(\nu)_4)=\sum_{n=m} a_6^n S_{\nu n}, \tag{19}$$

where

$$S_{\nu n}\equiv-\rho_1\omega^2 n_\nu\int_{\theta_c}^{\pi}P_\nu^m(\cos\theta)j_{q(n)}(k\tilde{R}(\theta))\times P_{q(n)}^m(\cos\tilde{\theta}(\theta))\sin\theta\,d\theta. \tag{20}$$

We will not list all the coefficients $t(\nu)_i$, their basic form can be found in the elastic equations for a shelled sphere (or as entries in the determinant of the system of equations) (see, for example, Refs. 3 and 4), but as an example we have

$$t(\nu)_2=\left[-2\nu\frac{(\nu+1)}{R}\left(-\frac{1}{R}j_\nu(k_{sh}^s R)+j_\nu'(k_{sh}^s R)\right)\right]a_5^\nu, \tag{21}$$

where R is evaluated at $R=a$ and a_5^ν is the coefficient in Eq. (6).

Similarly, for the radial displacement u_R we have from Eq. (8)

$$\sum_{n=m}^{N}(s(n)_1+s(n)_2+s(n)_3+s(n)_4)P_n^m(\cos\theta)$$

$$=\sum_{n=m}^{N}\frac{\partial}{\partial R}(j_{q(n)}(k\tilde{R})P_{q(n)}^m(\cos\tilde{\theta})),$$

$$\theta_c<\theta<\pi, \tag{22}$$

where $s(n)_i$ are the expressions for the four shell potential terms. Our approach is to multiply both sides of Eq. (22) by $P_k^m(\cos\tilde{\theta}(\theta))\sin(\tilde{\theta}(\theta))\partial\tilde{\theta}/\partial\theta$ and integrate with respect to θ where k corresponds to one of the possible values of q. Then we obtain

$$\sum_{n=m}^{N}(s(n)_1+s(n)_2+s(n)_3+s(n)_4)T_{\nu n}^m=\sum_{n=m}^{N}Q_{\nu n}^m, \tag{23}$$

where

$$T_{\nu n}\equiv\int_{\theta_c}^{\pi}P_{q(\nu)}^m(\cos\tilde{\theta}(\theta))P_n^m(\cos\theta)\sin\tilde{\theta}(\theta)\frac{d\tilde{\theta}}{d\theta}d\theta, \tag{24}$$

$$Q_{\nu n}\equiv\int_{\theta_c}^{\pi}P_{q(\nu)}^m(\cos\tilde{\theta}(\theta))\frac{\partial}{\partial R}[P_{q(n)}^m(\cos\tilde{\theta}(\theta))$$

$$\times j_{q(n)}(k\tilde{R})]\sin\tilde{\theta}(\theta)\frac{d\tilde{\theta}}{d\theta}d\theta. \tag{25}$$

Once again the general form of the coefficients can be found in Refs. 3 and 4, but as an example:

$$s(\nu)_2=\left[-\frac{1}{R}\nu(\nu+1)j_\nu(k_{sh}^s R)\right]a_5^\nu, \tag{26}$$

where R is evaluated at $R=a$.

In summary, for a fixed azimuthal order m, we take N_{in} unknown coefficients for the interior solution and N coefficients for each of the shell potentials and the exterior potential, obtaining a coupled $(5N+N_{in})\times(5N+N_{in})$ system of equations, with two of the continuity conditions at the inner interface providing the coupling mechanism. The condition Eq. (10) reduces to the standard noncoupled equation for the shell coefficients.

We now discuss an efficient method to compute the coupling integrals; the integrals T_{kn} are computed numerically and are independent of frequency. Thus they need to be computed only once if one is doing multiple frequency computations. The other integrals, S_{kn} and Q_{kn}, do depend upon frequency through the term $j_q(k\tilde{R})$ and thus it is advantageous to reexpress these integrands in terms of azimuthal (θ) terms which are frequency independent and frequency terms which do not depend upon θ; then the various azimuthal integrals need to be computed only once for multi-frequency computations. In order to reexpress these integrals we use the expressions for the translation of origins in spherical coordinate systems,[5,6]

$$j_q(k\tilde{R})P_q^m(\cos\tilde{\theta})=\sum_{n=m}^{\infty}C_{q,n}^m j_n(kR)P_n^m(\cos\theta), \tag{27}$$

where

$$C_{q,n}^m=(2n+1)\sum_{p=|q-n|}^{q+n}w_p(2p+1)(-i)^p j_p(kh)$$

$$\times i^{q-n}(-1)^m, \tag{28}$$

h is the vertical separation between the two origins and w_p is the product of Wigner-3j coefficients,

$$w_p=\begin{pmatrix}q & n & p\\ 0 & 0 & 0\end{pmatrix}\begin{pmatrix}q & n & p\\ m & -m & 0\end{pmatrix}\sqrt{\frac{(q-m)!(n+m)!}{(q+m)!(n-m)!}}. \tag{29}$$

References 5 and 6 use this type of representation for scattering from a pair of spheres; Lim[7] has also used the Wigner-3j representation to simplify his integrals for scattering in a multilayered acoustic medium. If the vertical offset of the center of the sphere from the origin is negative, then the result of Eq. (28) is multiplied by $(-1)^{q+n}$. Using these relationships in the definitions of Eq. (25) the various angular projection integrals can be expressed in terms of integrals which are independent of frequency. Thus, once again, these integrals are computed once and then repeatedly used in multiple-frequency computations.

III. NUMERICAL EXAMPLES

For the first example, a plane wave is incident on a sphere of radius 0.25 m with a 6-mm steel shell. The plane wave travels vertically along the z axis. Due to the azimuthal symmetry of the problem it is only necessary to compute the $m=0$ term of the solution. The level of the water fill in the sphere is varied as a fraction of the inner radius $R_a=0.244$ m. The plane wave is incident from the bottom so that it is initially incident upon the water in the sphere before encountering the water/air interface. Numerically, we investigated using different numbers of spherical harmonics in the computations. For the exterior and shell harmonics, the formula $N=1.5ka$ was used with a minimum number of eight harmonics used. This means that until approximately 5 kHz, 8 harmonics are used and this is increased linearly to 15 harmonics at the frequency of 10 kHz. For the interior basis functions it was found that for negative values of h (for those cases where the fraction of water fill is less than one-half) it was advantageous to use $N_{in}=N/2$ functions (one could use $N_{in}=N$, but for some frequencies there seemed to be numerically unstable results due to poor conditioning of the system of equations). It makes physical sense that less basis functions should be used for the case of small fractional fill since in this case the length of the water/shell boundary is relatively small. For values of fill greater or equal to one-half, the full number N was used (at a fraction of one-half, essentially the same results are obtained using either $N_{in}=N$ or $N_{in}=N/2$). As a check of the numerical accuracy of the method, we can consider the case of $h=R_a$ in which case the sphere is completely full of water. In Fig. 2 we show the resulting spectra as computed using the coupled-mode approach (solid) and using a standard harmonic expansion[3,4] for a fluid-filled sphere (dashed). In this computation a receiver is located in the backscatter direction, 10 m from the

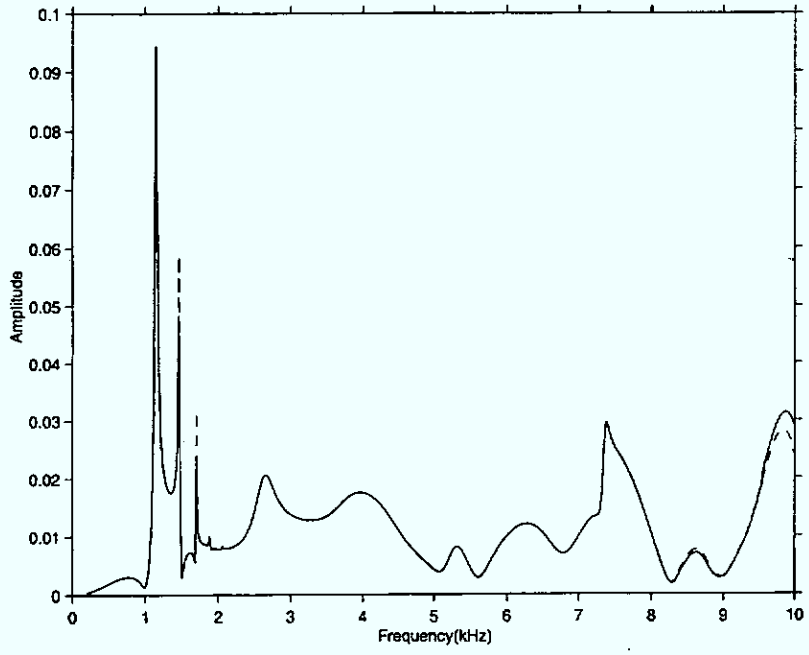

FIG. 2. A comparison between the exact (dashed) and computed (solid) spectra for the totally water-filled sphere.

center of the sphere. As can be seen the agreement is excellent. This is rather remarkable as the interior expansion for the coupled-expansion method is based upon an origin at the very top of the sphere. In Fig. 3 we show the resulting spectra for the backscattered energy starting with $h=-0.75R_a$ and ending with $h=0.75R_a$ in steps of $0.25R_a$. The first curve corresponds to the interior being almost empty and the last case to it being almost full. As the fill approaches the one-half fraction, it can be seen that the spectral levels for the higher frequencies increases significantly; this is due to the growing size of the water/air interface within the sphere. There is also a shifting of the resonance peaks in the 1–2 kHz range. At the $h=0.75R_a$ value a resonance peak can be seen at about $f=800$ Hz; although not shown in Fig. 3 this feature can be tracked for fill values less than this (e.g., $h=0.6R_a$ and starts to disappear as the sphere is filled more).

In Fig. 4 the corresponding time series for an incident 4-kHz Ricker pulse are shown. The incident pulse is still a plane wave but with a Ricker pulse shape in the time domain. The time series $p(t)$ is computed from the multi-frequency spectrum $S(\omega)$ using Fourier synthesis; in particular,

$$p(t)=2\Re\left\{\sum_{\omega_k} S(\omega)R(\omega)\Delta\omega e^{i\omega_k t}\right\}, \tag{30}$$

and $R(\omega)$ is the source spectrum,

$$R(\omega)\equiv\omega^2\exp(-\omega^2/\omega_c^2)\sqrt{\frac{2\pi}{\omega_c}}, \tag{31}$$

where in our example $\omega_c=2\pi 4000$. An important feature in Fig. 4 is that the strongest reflection comes from energy propagating in the sphere, hitting the water/air interface and

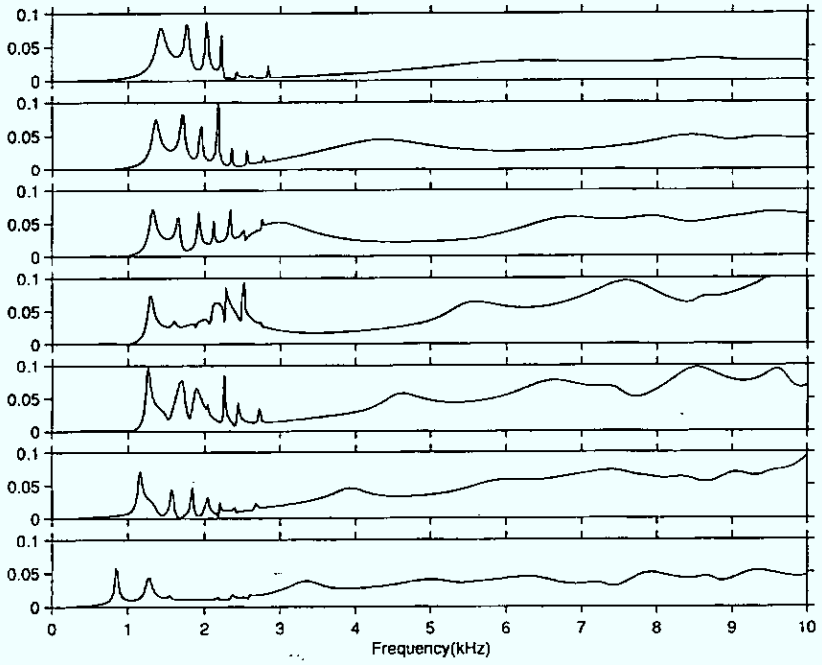

FIG. 3. The backscattered spectra as a function of fluid-fill: top curve is $h=-0.75R_a$ and bottom curve is $h=0.75R_a$ (varying from nearly empty to nearly full in steps of $0.25R_a$). The wave is incident from below (i.e., strikes water interior first).

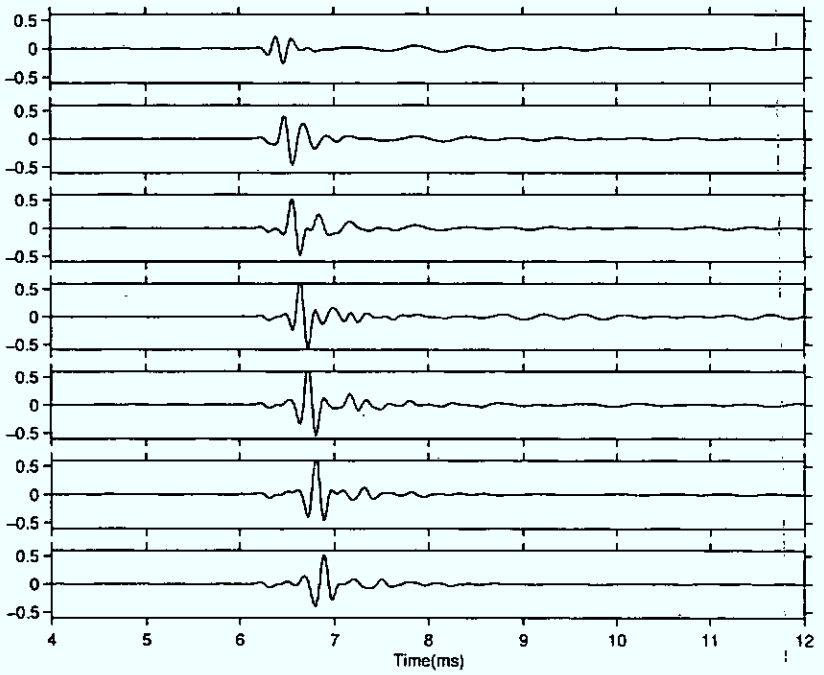

FIG. 4. The time series corresponding to the spectra of Fig. 3 for an incident 4-kHz Ricker pulse.

reflecting out. The amplitude of this reflection grows until $h=0$ or $h=0.25R_a$. This is reasonable as in this case the surface area of the water/air interface increases until $h=0$.

These computations are now repeated but for the plane wave incident from above, thus encountering the air-backed shell first. This is significantly different from the previous case in the sense that the incident wave cannot initially propagate in the interior of the sphere. The spectra for the various levels of fill and the corresponding time series are shown in Figs. 5 and 6. The top curves are for little fill ($h=-0.75R_a$) or equivalently for a large fraction of air. There is a noticeable variation in the spectra and time series as the amount of fill is changed, but there is no very large reflection from the water/air interface within the sphere as there was for the first set of curves (Figs. 2 and 3).

Finally, we consider a fixed frequency of 4 kHz, a fixed amount of fill ($h=0$ or the sphere is half-filled) and the monostatic scattering angle is varied; in this case it is necessary to compute the solution for varying values of m. For a sphere, totally fluid-filled or totally air-filled the scattering plot should be independent of the polar angle. However, as can be seen in Fig. 7, the polar plot for the half-filled case has a strong angular dependence.

IV. SUMMARY

It has been shown that the acoustic field scattered by a partially filled elastic-shelled sphere can be computed using a dual set of basis functions for the interior of the sphere and the shell and exterior of the sphere. The computations

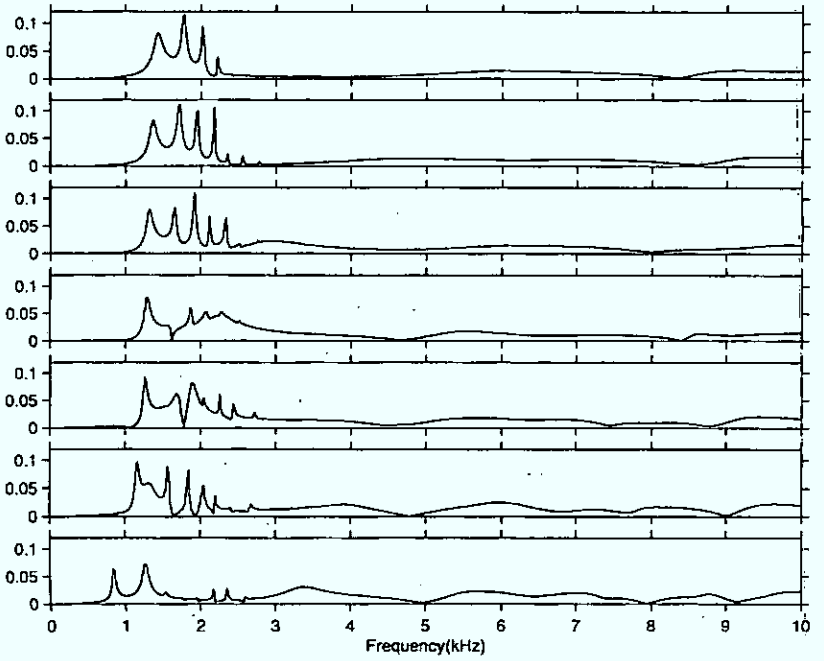

FIG. 5. The backscattered spectra as a function of fluid-fill: top curve is $h=-0.75R_a$ and bottom curve is $h=0.75R_a$ (varying from nearly empty to nearly full in steps of $0.25R_a$). The wave is incident from above (i.e., strikes air interior first).

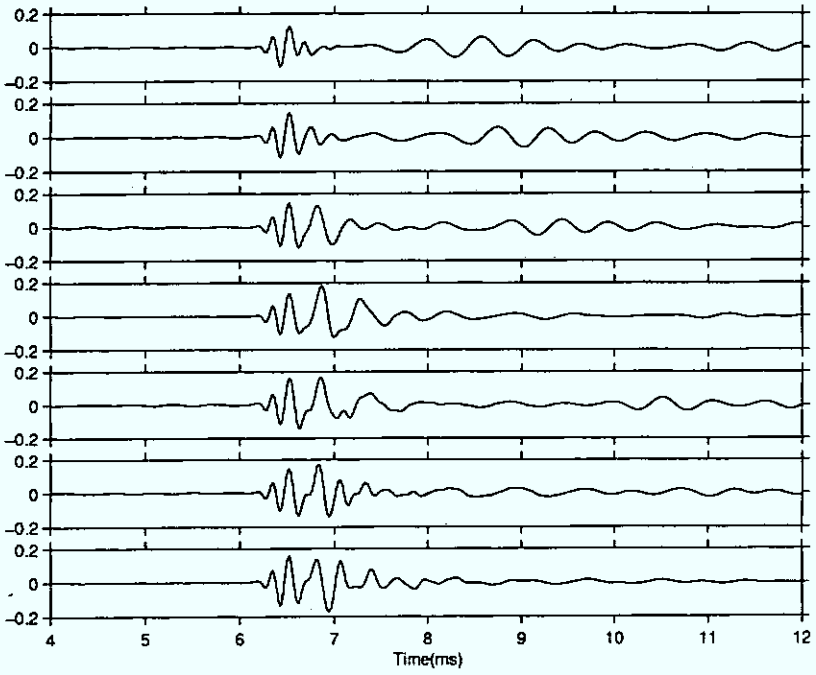

FIG. 6. The time series corresponding to the spectra of Fig. 5 for an incident 4-kHz Ricker pulse.

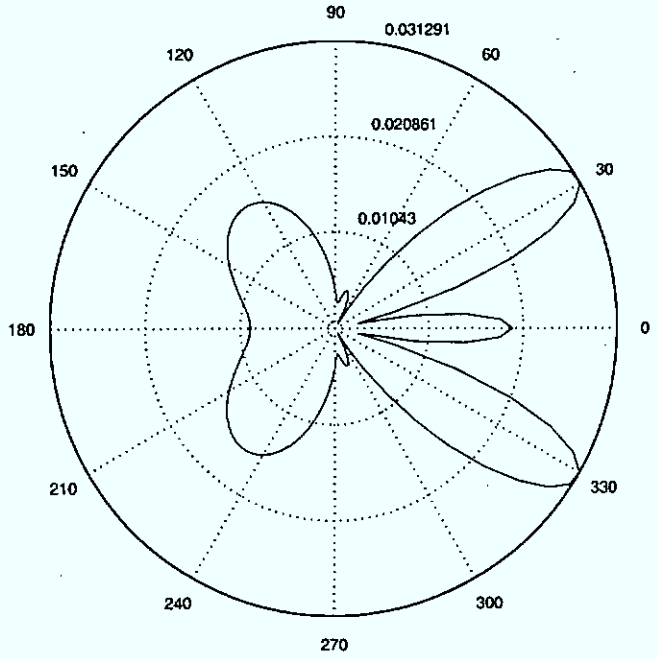

FIG. 7. A polar plot of monostatic backscattering level (receiver is 10 m from the sphere center) as a function of polar angle for a frequency of 4 kHz and the sphere is half-filled.

showed that partial fill could increase the target strength of the sphere for higher frequencies as the interior fluid/air interface became an increasingly strong scattering surface for a plane wave incident upon the fluid-fill. When the plane wave is incident upon the air-filled side, this effect is not so evident as the incident wave cannot propagate through the first part of the interior. The computations also showed how partial fill of the sphere makes the target scattering strength significantly angularly dependent.

[1]R. Hickling, "Analysis of echos from a hollow metallic sphere in water," J. Acoust. Soc. Am. **36**, 1124–1137 (1964).
[2]G. Kaduchak and C. Loeffler, "Relationship between material properties and target strength of fluid-filled spherical shells in water: calculations and observations," IEEE J. Ocean Eng. **23**, 26–30 (1998).
[3]G. C. Gaunaurd and M. F. Werby, "Lamb and creeping waves around submerged spherical shells resonantly excited by sound scattering," J. Acoust. Soc. Am. **82**, 2021–2033 (1987).
[4]G. C. Gaunaurd and M. F. Werby, "Sound scattering by resonantly excited, fluid-loaded, elastic spherical shells," J. Acoust. Soc. Am. **90**, 2536–2550 (1991).
[5]G. C. Gaunaurd, H. Huang, and H. C. Strifors, "Acoustic scattering by a pair of spheres," J. Acoust. Soc. Am. **98**, 495–507 (1995).
[6]J. Bruning and Y. Lo, "Multiple scattering of electromagnetic waves by spheres. Pt I. Multipole expansion an ray-optical solutions," IEEE Trans. Antennas Propag. **AP-19**, 378–390 (1971).
[7]R. Lim, "Multiple scattering by many bounded obstacles in a multilayered acoustic medium," J. Acoust. Soc. Am. **92**, 1593–1612 (1992).